LIQUEFACTION SEVERITY MAPS IN A PROBABILISTIC GROUND MOTION ENVIRONMENT FOR RICHMOND, BRITISH COLUMBIA, CANADA

Alireza Javanbakht, Sheri Molnar
Department of Earth Science, University of Western Ontario, London, Ontario, Canada

Abouzar Sadrekarimi
Department of Civil and Environmental Engineering, University of Western Ontario, London, Ontario, Canada

Sujan Adhikari
Department of Earth Science, University of Western Ontario, London, Ontario, Canada

ABSTRACT
Liquefaction hazard maps play an important role in site selection and planning stages for urban settlement and engineering structures. In this paper, probabilistic liquefaction severity maps of Richmond, British Columbia, Canada are presented considering ground motions corresponding to a probability of exceedance of 2% in 50 years based on the liquefaction potential index (LPI). Existing liquefaction hazard maps are produced using a single earthquake magnitude and its peak ground accelerations, while a seismic deaggregation method is used here to determine probabilistic LPI values. The factor of safety against liquefaction is calculated for 299 cone penetration tests (CPT) in an Excel spreadsheet using the most recent CPT-based liquefaction triggering methodology. The probabilistic liquefaction severity maps in this study are generated with two methods: geostatistical interpolation of LPI values and threshold LPI method based on the cumulative LPI distribution. The results show high liquefaction hazard in areas with an underlying thick sand layer and lower hazard in areas covered by peat deposits. The more cumbersome magnitude-distance deaggregation method generates similar results to using mean magnitude and thereby confirms the simpler applicability of mean magnitude in liquefaction hazard mapping of Richmond. In addition, sensitivity analyses indicate that LPI values are relatively sensitive to the groundwater table, particularly high LPI values.

RÉSUMÉ
Les cartes des risques de liquéfaction jouent un rôle important dans la sélection des sites et les étapes de planification des établissements urbains et des ouvrages d'art. Dans cet article, des cartes probabilistes de gravité de liquéfaction de Richmond, Colombie-Britannique, Canada sont présentées en considérant les mouvements du sol correspondant à une probabilité de dépassement de 2% en 50 ans basée sur l'indice du potentiel de liquéfaction (IPV). Les cartes des risques de liquéfaction existantes sont produites en utilisant une seule magnitude de séisme et ses accélérations de pointe au sol, tandis qu'une méthode de désagrégation sismique est utilisée ici pour déterminer les valeurs probabilistes de l'IPV. Le facteur de sécurité contre la liquéfaction est calculé pour 299 tests de pénétration de cône (CPT) dans une feuille de calcul Excel en utilisant la méthodologie de déclenchement de liquéfaction basée sur le CPT la plus récente. Les cartes probabilistes de gravité de la liquéfaction de cette étude sont générées avec deux méthodes: l'interpolation géostatistique des valeurs de l'IPV et la méthode du seuil d'IPV basée sur la distribution cumulative de l'IPV. Les résultats montrent un risque de liquéfaction élevé dans les zones avec une couche de sable épaisse sous-jacente et un risque moindre dans les zones couvertes par des dépôts de tourbe. La méthode plus lourde de désagrégation magnitude-distance génère des résultats similaires à l'utilisation de la magnitude moyenne et confirme ainsi l'applicabilité plus simple de la magnitude moyenne dans la cartographie des risques de liquéfaction de Richmond. De plus, les analyses de sensibilité indiquent que les valeurs de l'IPV sont relativement sensibles à la nappe phréatique, en particulier les valeurs d'IPV élevées.

1 INTRODUCTION

Liquefaction hazard mapping of prone regions is increasingly being incorporated into earthquake hazard mitigation practice. To prepare the liquefaction hazard map, a parameter predicting the hazard classification within each (surficial) geology unit is a requirement. Iwasaki et al. (1982) developed the liquefaction potential index (LPI) which determines the liquefaction potential (severity) along a soil profile from the ground surface to a depth of 20 m. The surface damages from liquefaction at depths greater than 20 m are rarely observed/reported. LPI is intended to be proportional to the amount by which the factor of safety against liquefaction is less than one (seismic demand larger than soil resistance and liquefaction will occur), and thickness and proximity of liquefied layers to surface. Many investigators have used LPI to categorize liquefaction hazard and generate liquefaction hazard maps (Toprak and Holzer 2003, Sonmez 2003, Hiedari and Andrus 2010, Rahman et al.

2015, Papathanassiou et al. 2017). Geotechnical *in-situ* tests such as cone penetration testing (CPT) and standard penetration test (SPT) are typically used to calculate LPI values. The advantage of using CPTs is their ability to measure thin potentially liquefiable layers that can be missed by SPT, and the high repeatability of CPTs (Robertson, 2004). Toprak and Holzer (2003) examined field observations of liquefaction from the 1989 Loma Prieta earthquake in comparison to LPI calculated using 50 CPTs at 20 sites. LPI values > 5 were correlated with the occurrence of sand boils and LPI values > 12 were correlated with lateral spreads occurrences. Holzer et al. (2006) presented a liquefaction hazard map based on cumulative frequency distributions of LPI per surficial geologic unit based on CPT and SPT measurements along the eastern shore of San Francisco Bay, including the city of Oakland. Lenz and Baise (2007) investigated CPT- and SPT-based liquefaction potential considering LPI criteria across the East San Francisco Bay and demonstrated the use of kriging as a geostatistical method to interpolate between LPI data points to generate liquefaction hazard maps. Kim et al. (2020) applied LPI to predict local and regional sand boils and the calculated values were in good agreement with field observations of liquefaction damage from a magnitude (M) 5.4 earthquake in Pohang, South Korea. Bahari et al. (2020) investigated liquefaction probability considering deterministic and reliability methods and generated liquefaction hazard maps of Eco-Delta city in the southwestern part of Busan, South Korea. Particular to Metropolitan Vancouver, British Columbia, Monahan et al. (2010a) generated a liquefaction hazard map of Richmond using the probability of liquefaction severity (PLS) index and considering a deterministic M 7 earthquake scenario.

In this study, liquefaction severity hazard maps of Richmond, British Columbia, Canada based on probabilistic LPI are presented corresponding to the ground motions for a probability of exceedance (PE) of 2% in 50 years applying the magnitude-distance deaggregation method (Finn and Wightman 2007; Finn et al. 2016) to evaluate liquefaction triggering. This paper builds on previous liquefaction susceptibility mapping for western Metro Vancouver (A. Javanbakht, pers. comm., 2019) and seismic-induced liquefaction hazard mapping for Richmond considering a M 7.5 earthquake scenario (Javanbakht et al. 2021). The maps are generated with two methods: the LPI threshold method and geostatistical LPI interpolation. In addition, probabilistic LPI values predicted from magnitude-distance deaggregation analyses are compared with those from mean magnitude application, both using the 2% PE in 50 years PGA. In the last section of this paper, the sensitivity analysis of LPI values to the groundwater table (GWT) is presented. Probabilistic liquefaction potential (severity) maps for Richmond presented in this paper are part of the Metro Vancouver seismic hazard mapping project (Molnar et al. 2020). The Institute for Catastrophic Loss Reduction (ICLR) and the University of Western Ontario with support from Emergency Management British Columbia (EMBC) are working together to generate comprehensive earthquake hazard maps for the Metro Vancouver region of British Columbia (https://metrovanmicromap.ca).

2 ENGINEERING GEOLOGY AND CPT DATA OF RICHMOND

The study region includes Richmond city with an area of 129 km^2 located entirely within the Fraser River Delta in southwestern British Columbia. The deltaic deposits underlie Richmond with variable thickness from less than 20 m to a maximum of 305 m at Richmond City Hall (Monahan et al. 2010b). The topset of the deltaic section deposited on the delta plain contains sand, silt, and locally peat. Topset deposits are dominated by sands with a thickness of 8-30 m. Older sand facies are located below a thicker layer of organic silt with peat near the ground surface. The geological variation in the Quaternary deposits underlying Richmond has been mapped by Monahan et al. (2010b), shown in Figure 1, based on a combination of surface and subsurface information from boreholes deeper than 10 m and CPTs.

The sF unit (Fig. 1) is widespread in western Richmond and contains thick sand facies of 8 to 25 m, present at relatively shallow depths (within upper 7 m). Foreset deposits underlie the sand facies in this unit. The subunits of sF have the same characteristics except where mentioned otherwise: the sF1 unit exists along the North Arm of the Fraser River with topset sand layers directly overlying overconsolidated Pleistocene deposits rather than deposits of the foreset, the sF2 unit occurs between units sF1 and sF, the sF3 is located in the western Richmond with sand facies and interbedded sand and silt facies, the sFy unit comprises areas with topset young sands and is found on the riverside of a series of sloughs in southwest of the delta. The szF unit is assigned to the interbedded sand and silt facies with thickness of 20 m and large occurrence along the Main Channel of the Fraser River. The subunit szF1 contains thick silts with minor interbedded sands. The O* unit represents areas with peat layers at the surface and topset sands at depth of less than 10 m and occurs widely in central Lulu Island. This unit is subdivided into eastern Oe* and western Ow* units. The zO* unit includes silts overlying peat, while the szO* unit is interbedded sands and silts overlying peat. The sO* and hzF* units represent thin sand overlying peat and moderately thick organic silts, respectively. The surface peat and thick organic silts with sand facies at depth of greater than 10 m (usually from 10 m to 20 m) are shown with unit O and it is also subdivided into east (Oe) and west (Ow) subunits. All other Quaternary geologic unit descriptions can be found in Monahan et al. (2010b).

A total number of 299 CPT soundings are present in the Richmond area (Figure 1) from our compiled regional geodatabase (Adhikari et al. 2021a) and are used in our LPI analyses. Of the 299 CPT soundings, 245 (84%) have a depth greater than 20 m. Of the soundings that do not reach 20 m, 33 CPT profiles terminate at 15-20 m and 21 CPTs reach depths of 10-15 m. 194 CPTs (65%) are accompanied by one borehole with laboratory testing providing fines content, grain size distribution, water content, and plasticity.

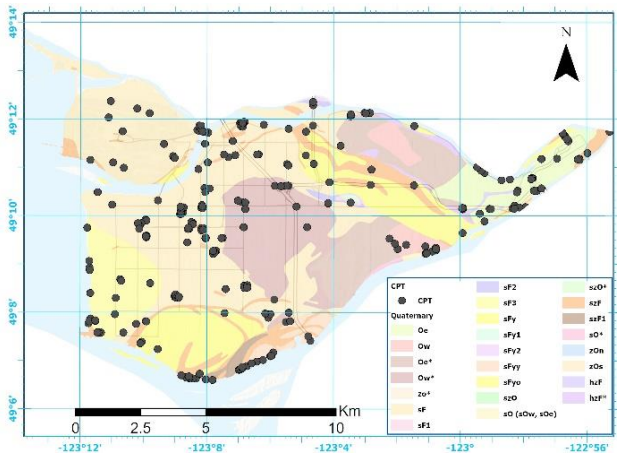

Figure 1. The Quaternary geological map of Richmond (Monahan et al. 2010b) with CPT locations (circles).

The number of CPT profiles are normalized by area underlain by each geology unit and shown in Figure 2. The sO unit has the greatest CPT density (7 CPT within 0.3 km^2), while hzF* and Oe* show the lowest.

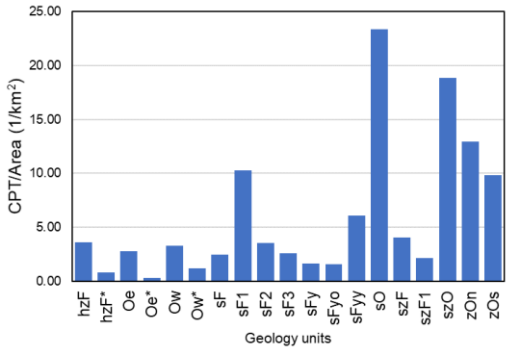

Figure 2. Histogram of CPT data within geology units of Richmond.

3 CPT-BASED METHODOLOGY TO DETERMINE LPI IN A PROBABILISTIC FRAMEWORK

Because the maximum depth for LPI calculation along CPT profile is limited to 20 m, the simplified method is used in this study to obtain the factor of safety (FS) against liquefaction. The cone resistance (q_c), sleeve friction resistance (f_s), and water pore pressure behind the cone (u_2) were extracted from the 299 CPT profiles to use in the simplified procedure to calculate FS. The factor of safety for each soil layer in the simplified procedure is defined as the ratio of cyclic resistance ratio (CRR) to cyclic stress ratio (CSR). The CRR is the resistance provided by the soil, dependent on soil type, stress level, fines content, initial shear stress and density determined from geotechnical (*in situ* and laboratory) testing and the CSR is a measure of the earthquake demand.

In preparation to calculate CRR, the groundwater table (GWT) is inferred from *in situ* tests if reported, otherwise, it would be obtained from a regionally interpolated map of groundwater table for the Greater Vancouver area (Adhikari et al. 2021a). Soil above the groundwater table would not liquefy. The effect of GWT on LPI values is investigated further in the last section of this paper. The measured cone resistance is corrected for pore water pressure acting on the cone (u_2) to obtain corrected cone resistance, q_t. For sandy soils, the magnitude of this correction is small, while in soft clay layer is significantly large. In our analyses, pore water correction is applied whenever the value of u_2 is measured and we use the term q_c with the understanding that the correction has been performed.

For defining the soil type of each layer from CPT measurements, the soil behavior type index (I_c) proposed by Robertson and Cabal (2015) is used. I_c is calculated via normalized cone resistance and sleeve friction ratios considering the stress exponent ^{n} which changes from 0.5 in sands to 1.0 in clays. In this paper, if I_c is greater than 2.60, then the soil has too much fines content (too clayey) to liquefy. However, Youd et al. (2001) suggest that soil layers with I_c > 2.4 should be sampled and tested to investigate the soil behavior type.

The q_c term is corrected for overburden stress by applying C_N overburden correction factor of Boulanger (2003) which requires an iterative procedure in our Excel spreadsheet. The normalized tip resistance for silty sands should be corrected to an equivalent clean sand term (q_{c1Ncs}). The equivalent clean sand adjustment, Δq_{c1N} is considered in this simplified method for the effect of fines content (FC) on cyclic stress ratio and cone penetration resistance from Boulanger and Idriss (2016). Δq_{c1N} and q_{c1Ncs} are estimated from Eqs. (1 and 2):

$$\Delta q_{c1N} = \left(11.9 + \frac{q_{c1N}}{14.6}\right) \exp\left(1.63 - \frac{9.7}{FC+2} - \left(\frac{15.7}{FC+2}\right)^2\right) \quad (1)$$

$$q_{c1Ncs} = q_{c1N} + \Delta q_{c1N} \quad (2)$$

Fines content (FC) is obtained from adjacent boreholes if it is reported, otherwise, it is estimated from a correlation with I_c by Boulanger and Idriss (2016). Noting the estimation of FC from this correlation can be problematic. Cyclic resistance ratio (CRR) is computed from the latest methodology by Boulanger and Idriss (2016) shown in Eq. (3):

$$CRR_{M=7.5,\sigma'_v=1atm} = \exp\left(\frac{q_{c1Ncs}}{113} + \left(\frac{q_{c1Ncs}}{1000}\right)^2 - \left(\frac{q_{c1Ncs}}{140}\right)^3 + \left(\frac{q_{c1Ncs}}{137}\right)^4 - 2.80\right) \quad (3)$$

The average CSR for each soil layer of the 299 CPT soundings is calculated from the well-known formula by Seed and Idriss (1971) from Eq. (4):

$$CSR = \frac{\tau_{av}}{\sigma'_{v0}} = 0.65\left(\frac{a_{max}}{g}\right)\left(\frac{\sigma_{v0}}{\sigma'_{v0}}\right)\frac{r_d}{MSF} \quad (4)$$

where a_{max} is the peak ground acceleration, g is the acceleration of gravity, r_d is the stress reduction factor proposed by Idriss (1999) in extending the work of Golesorkhi (1989), σ_{v0} and σ'_{v0} are total and effective vertical stresses respectively at the depth of interest, τ_{av} is average cyclic shear stress, and MSF is magnitude scale factor. The revised MSF by Boulanger and Idriss (2016) is applied in this paper in evaluating liquefaction triggering

potential as it extends to magnitude 9 and considers Cascadia event in the simplified estimation of FS. The Boulanger and Idriss (2016) MSF will produce higher CSR for small earthquake magnitudes. The MSF is obtained from Eq. (5):

$$MSF = 1 + (MSF_{max} - 1)[8.64 \exp\left(\frac{-M_w}{4}\right) - 1.325 \quad (5)$$

$$MSF_{max} = 1.09 + (\frac{q_{c1Ncs}}{180})^3 \leq 2.2 \quad (6)$$

Hence, the simplified method for defining CSR is a deterministic approach with a single moment magnitude which tends towards the maximum magnitude and its peak ground acceleration (PGA) for the site. Considering only a single maximum magnitude in simplified procedure does not account for contributions of all magnitudes to probabilistic a_{max}. One method to calculate the factor of safety is a procedure based on a magnitude-distance deaggregation (Finn and Wightman 2007; Finn et al. 2016) which is performed in this study to take into account all magnitude contributions to a probabilistic PGA with a 2% PE in 50 years. Finn and Wightman (2007) determined the deaggregation method is equivalent to a fully probabilistic liquefaction analysis or use of mean magnitude with the 2% PE in 50 years PGA.

Seismic source deaggregation is performed in Richmond (49.16785^{0}N, 123.16879^{0}W, immediately south of Sea Island) using CanadaSHM6 input files (Kolaj et al., 2020) for a V_{s30} of 160 m/s to understand the magnitude-distance contributions and mean magnitude using the GEM OpenQuake engine (Adhikari et al. 2021b) and the results are shown in Figure 3. The bar graph shows the contribution to probabilistic PGA from each magnitude (0.1) and distance (20 km) bins. It should be noted that there is no significant contribution from distances farther than 200 km. The contribution of the bin magnitudes is sampled at various distances and shown by row numbers in the magnitude contribution matrix. The total contribution from each magnitude is obtained from this matrix. Figure 4 shows the contribution of each deaggregated magnitude to a probabilistic a_{max} for Richmond. The sum of the contributions is 100%. There are no contributions from earthquakes with M_w=7.7-8.4 due to the use of a maximum distance of 400 km for the active shallow crust, and, subduction interslab, 600 km for the stable shallow crust and 1000 km for subduction interface.

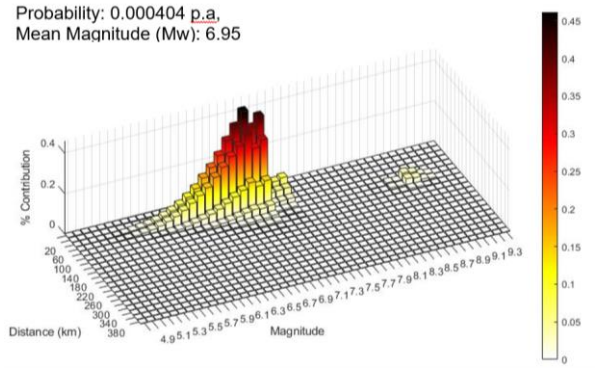

Figure 3. Magnitude-distance deaggregation for a select location in Richmond.

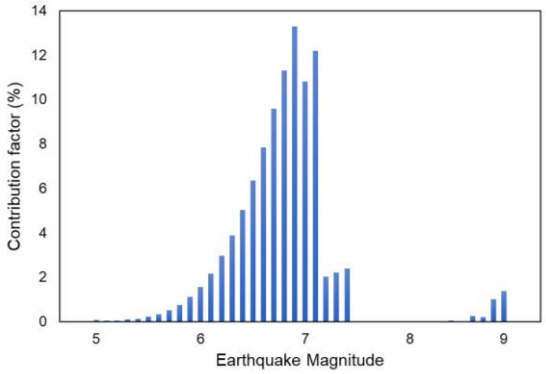

Figure 4. Contributions of deaggregated magnitudes to probabilistic PGA in Richmond.

Table 1 shows an example of how we applied deaggregation in the simplified procedure to calculate the safety factor against liquefaction for each soil layer. The FS is computed for each bin magnitude (considering the central magnitude in the bin) and then multiplied by the contribution factor of that magnitude from Figure 4. The global FS is the summation of FS from all bins. For this example, the global FS is 0.439.

Table 1. Sample calculation of global FS for a soil layer at depth of 5 m with q_{c1N} = 70.

Magnitude bins	Central magnitude	Liquefaction FS	Contribution factor	Weighted FS
5.0-5.1	5.05	0.607	0.0007	0.0004
5.1-5.2	5.15	0.595	0.0004	0.0002
5.2-5.3	5.25	0.584	0.0006	0.0003
5.3-5.4	5.35	0.572	0.0009	0.0005
5.4-5.5	5.45	0.561	0.0014	0.0007
5.5-5.6	5.55	0.551	0.0022	0.0121
5.6-5.7	5.65	0.540	0.0034	0.0018
5.7-5.8	5.75	0.530	0.0052	0.0027
5.8-5.9	5.85	0.520	0.0076	0.0040
5.9-6.0	5.95	0.510	0.0111	0.0002
6.0-6.1	6.05	0.501	0.0157	0.0056
6.1-6.2	6.15	0.492	0.0217	0.0107
6.2-6.3	6.25	0.483	0.0296	0.0143
6.3-6.4	6.35	0.474	0.0388	0.0184
6.4-6.5	6.45	0.466	0.0503	0.0234
6.5-6.6	6.55	0.458	0.0635	0.0291
6.6-6.7	6.65	0.450	0.0784	0.0353
6.7-6.8	6.75	0.442	0.0959	0.0424
6.8-6.9	6.85	0.434	0.1130	0.0490
6.9-7.0	6.95	0.427	0.1330	0.0568
7.0-7.1	7.05	0.420	0.1080	0.0454
7.1-7.2	7.15	0.413	0.1220	0.0504
7.2-7.3	7.25	0.406	0.0202	0.0082
7.3-7.4	7.35	0.399	0.0222	0.0086
7.4-7.5	7.45	0.393	0.0239	0.0094
7.5-7.6	7.55	0.386	0.0001	0.0000
7.6-7.7	7.65	0.380	0.0001	0.0000
7.7-7.8	7.75	0.374	0.0000	0.0000
7.8-7.9	7.85	0.368	0.0000	0.0000
7.9-8.0	7.95	0.363	0.0000	0.0000
8.0-8.1	8.05	0.357	0.0000	0.0000
8.1-8.2	8.15	0.352	0.0000	0.0000
8.2-8.3	8.25	0.346	0.0000	0.0000
8.3-8.4	8.35	0.341	0.0000	0.0000
8.4-8.5	8.45	0.336	0.0004	0.0001
8.5-8.6	8.55	0.331	0.0001	0.0000
8.6-8.7	8.65	0.326	0.0026	0.0009
8.7-8.8	8.75	0.322	0.0020	0.0006
8.8-8.9	8.85	0.318	0.0101	0.0032
8.9-9.0	8.95	0.314	0.0138	0.0043
			Σ=1.0	FS=0.439

The described CPT-based methodology by Boulanger and Idriss (2016) in a probabilistic framework applying the magnitude-distance deaggregation method combined with probabilistic PGA with a 2% PE in 50 years is then applied for all of Richmond. FS is computed at 0.05 m depth intervals in 299 CPT profiles for over 96,000 soil layers and 62% of calculated FS are less than 1 (liquefiable) which results in high LPI values throughout Richmond. The same deaggregated magnitude weightings (matrix) in Figure 4 are applied to all CPT locations. Lateral variability in probabilistic a_{max} is less than CRR at this municipal level scale and generally decreases eastward. Future work will consider variability in probabilistic a_{max} across Metro Vancouver.

4 DETERMINATION OF LPI

LPI closely represents the consequence of liquefaction at ground surface and is obtained from Eq. (7):

$$LPI = \int_0^{20} F_L w(z) dz \quad (7)$$

where

$$F_L = 1 - FS \qquad FS \leq 1 \quad (8a)$$

$$F_L = 0 \qquad FS > 1 \quad (8b)$$

and w(z)=10-0.5z, where z is depth.

The weighting factor, w(z), is a linear function of depth and it changes from 10 at the ground surface to 0 at a depth of 20 m. The factor of safety against liquefaction was calculated for all CPT profiles based on the methodology explained in the previous section and we use the discretized form of LPI proposed by Luna and Frost (1998) for continuous CPT soundings. The LPI values then range from 0 to 100 and the LPI classification proposed by Iwasaki et al. (1982) is used to map seismic-induced liquefaction potential Richmond; very low (LPI = 0), low (0 < LPI ≤ 5), high (5 < LPI ≤ 15) and very high (LPI > 15). The histogram of Figure 5 shows that 247 calculated LPIs are greater than 15 (very high hazard), while only 27 LPIs are categorized into low hazard (≤ 5). The distribution of these LPIs across Richmond are presented in Figure 6. Most of the LPI values are > 15 showing very high hazard span in much of western and central Lulu Island whereas LPIs classified into low hazard (≤5) occur primarily in eastern Richmond.

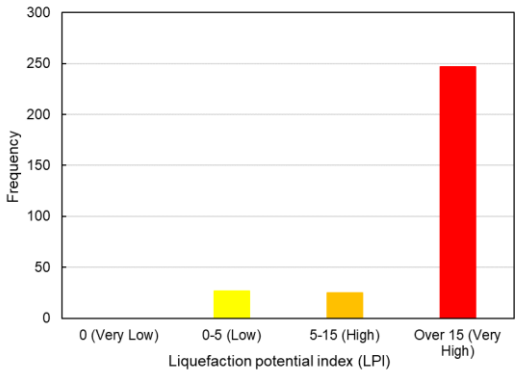

Figure 5. Histogram of calculated LPI values for Richmond.

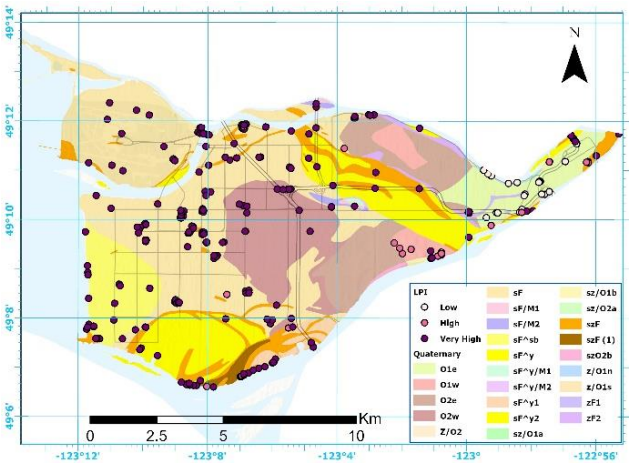

Figure 6. LPI values distribution across Richmond.

5 LIQUEFACTION HAZARD MAPPING

We use two methods to generate liquefaction potential hazard maps for Richmond. The first method is based on direct geostatistical interpolation of probabilistic LPIs of the previous section. This method disregards geological boundaries and works well with good spatial coverage and density of LPI values such as in Richmond but may not be as applicable elsewhere in Metro Vancouver. The second method uses thresholds determined from the cumulative frequency of LPI within each geology unit. The requirement for cumulative distribution of LPI method is the assumption of statistical homogeneity within a geology unit, however, liquefaction potential can vary within a mapped geology unit (Terzaghi, 1995). It should be noted that the true liquefaction hazard map is coming from the combination of direct interpolation and geological boundaries. This means that we will need sufficient data for each geology unit to apply the direct interpolation within each geology unit.

5.1 INTERPOLATED PROBABILISTIC LPI MAPPING

The kriging interpolation technique is applied to estimate interpolated values of probabilistic LPI from neighborhood points and produce a spatially interpolated liquefaction hazard map. Figure 7 shows the liquefaction hazard map of Richmond based on interpolation of probabilistic LPI considering the contribution of a wide range of earthquake magnitudes (M 5-9) at a 2% PE in 50 years. Almost all regions in the west, north and central parts of the city were found to have very high hazard of liquefaction. The young sand layers in southern Richmond relate to very high hazard of liquefaction. Other factors that contribute to high and very high hazard is thick layers of interbedded sand layers combined with a shallow water table level in the region. In eastern Richmond, peat layers varying from 1 to 10 m thick result in low liquefaction hazards. The peat layers are not liquefiable (act as an impenetrable layer) even with very low cone resistance. As former/current bog areas, there is very little topographic relief to permit lateral spreading (breakage) of the peat to allow lower liquefied sands to reach the surface.

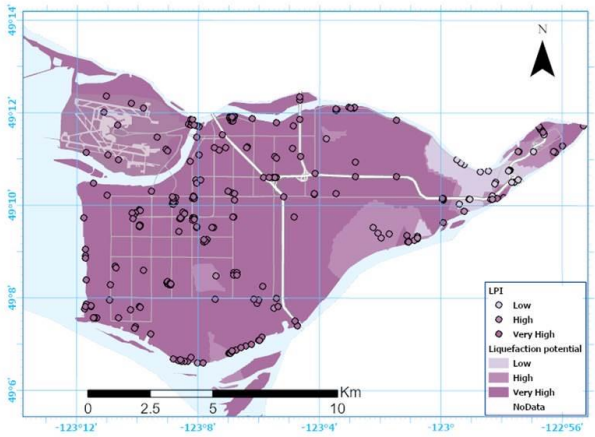

Figure 7. Liquefaction hazard map of Richmond with LPI in a probabilistic framework for probabilistic PGA with a 2% PE in 50 years.

5.2 LPI THRESHOLD MAPPING

Holzer et al. (2006) proposed that surface manifestation of liquefaction occurs when LPI is ≥ 5 and we use this criterion as the threshold for probability of moderate liquefaction within each geological unit. Iwasaki et al. (1982) concluded that the LPI ≥ 15 correlates with severe liquefaction effect at the ground surface. We apply this LPI threshold to define the probability of severe liquefaction. Sand boil is a consequence of moderate damage from liquefaction, while severe liquefaction results in damages such as lateral spreads.

Figure 8 presents a histogram for four selected geology units including Oe, szF, sF, sF3 units. The probability of moderate and severe liquefaction for Oe unit is zero, while szF has a 98% chance of moderate liquefaction damage (LPI ≥ 5) and a 78% probability of major damages from liquefaction (LPI ≥ 15). The probability of severe and moderate liquefaction within sF unit is 97% and 100%, respectively. The sF3 unit shows a 100% probability of moderate and severe liquefaction.

The probability of moderate liquefaction and severe liquefaction for all geology units were determined from the discussed method and liquefaction potential maps were generated for two probabilistic LPI thresholds (LPI ≥ 5, LPI ≥ 15). Figure 9 shows a liquefaction hazard map of Richmond at the threshold of moderate liquefaction damage such as sand boils considering probabilistic PGA at 2% in 50 years. Almost all geology units have a high probability of sand boil damages. Surface manifestations of liquefaction are not anticipated within the geology units east of Richmond containing thick peat and silt layers.

The liquefaction severity map (LPI ≥ 15) with surface damages such as lateral spreads considering probabilistic PGA at 2% PE in 50 years is presented in Figure 10. Areas in east Richmond would not suffer from severe damages from liquefaction (zero probability), but all other areas are predicted to have over 50% probability of severe liquefaction damages. The 97% and 100% probabilities of severe liquefaction are anticipated over large portions of central and northern Richmond including the Vancouver international airport on Sea Island.

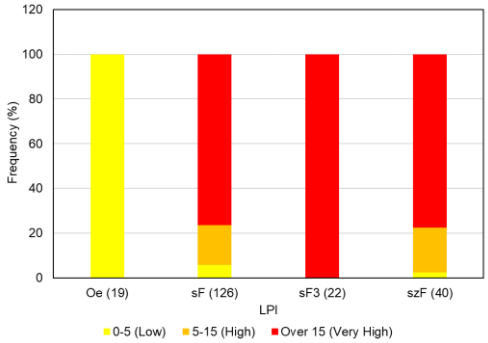

Figure 8. Histogram showing hazard classification based on LPI values within four geology units. Numbers within the parentheses show the CPT soundings.

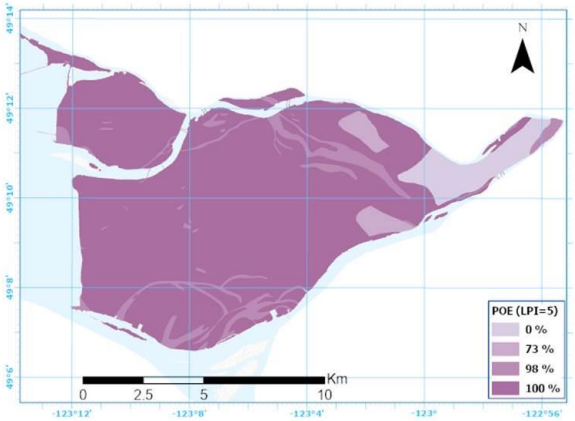

Figure 9. Probability of moderate liquefaction (LPI ≥ 5), e.g., surface manifestation of sand boils, for Richmond at 2% PE in 50 years.

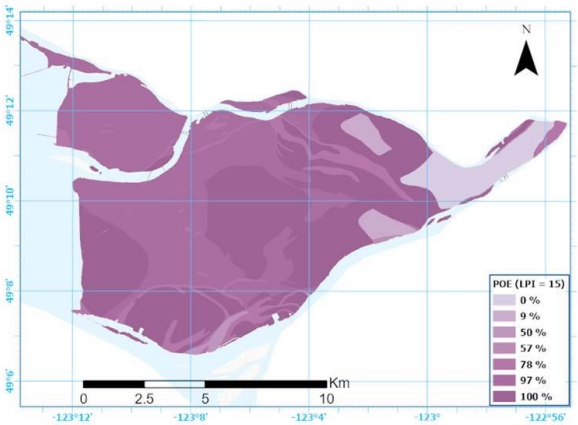

Figure 10. Probability of severe liquefaction (LPI ≥ 15), e.g., surface manifestation of lateral spreading, for Richmond at 2% PE in 50 years.

6 EVALUATION OF PROBABILISTIC LPI

The magnitude deaggregation method is applied in the simplified procedure to determine probabilistic LPI. This is a cumbersome approach compared to a single deterministic earthquake scenario. In this section, the FS and LPI values from the magnitude deaggregation method

are compared with simply using the mean magnitude of Richmond (6.95 from Fig. 3) obtained by the magnitude deaggregation analysis with probabilistic a_{max}. Table 2 shows FS for different q_{c1N} at one CPT location from the magnitude deaggregation and mean magnitude methods. There is a little difference between computed values from both methods which means that the simpler mean magnitude method to calculate FS is applicable for Richmond.

Table 2. Comparing FS from magnitude deaggregation method and mean magnitude for Richmond.

q_{c1N}	FS from magnitude deaggregation method	FS from mean magnitude
55	0.18	0.18
65	0.21	0.20
93	0.25	0.24
128	0.37	0.36
138	0.50	0.48
172	1.25	1.18

The median LPI values for all CPT profiles are recalculated using mean magnitude application and compared in Figure 11 with those previously calculated using the magnitude deaggregation method for each geology unit. The results show an insignificant difference between the two methods in calculating probabilistic LPI. Liquefaction hazard maps considering mean magnitude and probabilistic PGA would be the same as those determined using the magnitude-distance deaggregated methodology and probabilistic PGA. The simpler mean magnitude approach for generating a liquefaction severity map of Richmond is recommended for practice.

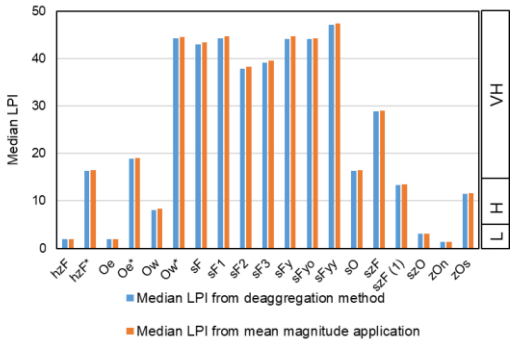

Figure 11. Comparing median LPI values from magnitude deaggregation method and mean magnitude application.

7 EFFECT OF GROUNDWATER TABLE

In this study, the groundwater table (GWT) is used directly from *in situ* tests if reported, otherwise, it is obtained from a regional groundwater table map for Greater Vancouver area (Adhikari et al. 2021a). However, the water table level varies by season, year, or even longer-term climate change. Raising the GWT increases the CSR through the ratio of vertical total and effective stresses and thereby decreases FS. In addition, in most areas of Richmond, liquefiable thick sand layers are commonly found at shallow depths and when the GWT rises towards the ground surface there will be an increase in liquefaction susceptible soil layers in LPI calculations. In addition, because LPIs are weighted more in the near surface (10 m) than at depth (0 at 20 m), increased saturation in shallower layers will cause a significant increase in LPI. Therefore, groundwater table plays an important role in generating liquefaction hazard maps and can significantly alter liquefaction hazard predictions.

To evaluate the importance of GWT, adjustment of $\pm$1 m to the original GWT depth is performed and the LPIs at each site are recalculated. For reference, it is expected that GWT will rise 0.5 m in the next 50 years (http://www.fraserbasin.bc.ca). Figure 12 shows the cumulative LPI distribution for original GWT, GWT+1m and GWT-1m. For the original GWT, 90% of LPIs are > 5 and 82% of LPIs are > 15. When the water table is considered more closely to ground surface (GWT-1m), 93% of calculated LPIs are classified into very high and high hazard (> 5) and 85% of LPIs are categorized into very high hazard (> 15). The spread between cumulative LPI functions increases with increasing LPI, readily demonstrating that higher LPIs are more sensitive to GWT changes.

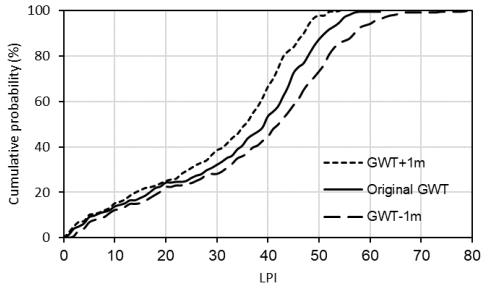

Figure 12. Sensitivity of LPI values to GWT changes.

8 CONCLUSION

The Metro Vancouver seismic microzonation hazard mapping project is generating regional liquefaction hazard map product(s) (Javanbakht et al. 2021). This paper documents probabilistic liquefaction severity mapping for Richmond, a case study example in terms of methodologies and map metrics towards wider application in future for Metro Vancouver. We applied the magnitude deaggregation method to a simplified procedure to consider the contributions of a wide range of magnitude to probabilistic PGA. The probabilistic LPIs were computed for 299 CPT sites. Most areas of Richmond are categorized into high and very high hazard of liquefaction and will exhibit surface manifestation of liquefaction considering the region's seismic hazard (PGA at a 2% PE in 50 years). In eastern Richmond, liquefaction hazard is determined to be low and surface damage from liquefaction is not predicted to be observed considering a 2% PE in 50 years PGA shaking level due to thick layers of non-liquefiable peat. A simpler mean magnitude approach to calculating probabilistic LPI results in similar LPI values as the more cumbersome deaggreation method and confirms applicability using of mean magnitude with probabilistic

PGA in future for Metro Vancouver. The LPIs, particularly high values, are sensitive to GWT fluctuations and can change significantly. Future work should consider improved accuracy in GWT throughout Metro Vancouver for regional liquefaction hazard mapping.

9 ACKNOWLEDGMENTS

We gratefully acknowledge multiple agencies, organizations, municipalities, and individuals that provided both public and private sources of CPT data to the Metro Vancouver seismic microzontion project. Funding is provided by the Institute for Catastrophic Loss Reduction (ICLR) with support from Emergency Management British Columbia (EMBC).

10 REFERENCES

Adhikari, S.R., Molnar S.E. and Wong, J. 2021a. Significance of Geodatabase Development for Seismic Microzonation in Metropolitan Vancouver, Canada, *17th World Conference on Earthquake Engineering*, Sept. 28th-October 2nd, 2021, Sendai, Japan, Paper No: 4521, 12 pgs.

Adhikari, S. R., Molnar S.E. and Wang, J. 2021b. Region specific Vs_{30} across Metro Vancouver and impact to seismic design ground motions, *Canadian Geotechnical Society annual meeting*, Sept. 26-29, 2021, Niagara, ON, Paper ID61, 8 pgs.

Bahari, B., Hwang, W., Kim, T.H. and Song, Y.S. 2020. Estimation of Liquefaction Potential in Eco-Delta City (Busan) Using Different Approaches with Effect of Fines Content, *Geo-Eng.*, 11: p. 14.

Boulanger, R.W. 2003. High Overburden Stress Effects in Liquefaction Analyses, *J. Geotechnical and Geoenvironmental Eng*., ASCE 129 (12): 1071–082.

Boulanger, R.W. and Idriss, I.M. 2016. CPT-Based Liquefaction Triggering Procedure, *J. Geotech. Geoenviron. Eng.*, 142 (2), 11.

Finn, W.D.L. and Wightman, A. 2007. Logical Evaluation of Liquefaction Potential Using NBCC 2005 Probabilistic Acceleraitons, In: *Proceedings of the ninth Canadian conference on earthquake engineering*, Ottawa, Ontario, Canada, 1894–1993.

Finn, W.D.L., Dowling, J. and Ventura, C.E. 2016. Evaluating Liquefaction Potential and Lateral Spreading in a Probabilistic Ground motion, *environment Soil Dyn. Earthq. Eng.*, 91: 202-208.

Golesorkhi, R. 1989. Factors Influencing The Computational Determination of Earthquake-Induced Shear Stresses in Sandy Soils, Ph.D. thesis, University of California at Berkeley, 395 pp.

Heidari, T. and Andrus, R.D., 2010. Mapping Liquefaction Potential of Aged Soil Deposits in Mount Pleasant, *South Carolina Engineering Geology*, 112 (1): 1-12.

Holzer, T. L., Bennett, M.J., Noce, T.E., Padovani, A.C. and Tinsley, J.C. 2006. Liquefaction Hazard Mapping with LPI in the Greater Oakland, California, Area, *Earthquake Spectra*, 22 (3): 693–708.

Idriss, I.M. 1999. An Update to the Seed-Idriss Simplified Procedure for Evaluating Liquefaction Potential, In Proceedings, TRB Workshop on New Approaches to Liquefaction, Publication No. FHWARD-99-165, Federal Highway Administration, January.

Iwasaki T., Tokida, K., Tatsuoka, F., Watanabe, S., Yasuda, S. and Sato, H. 1982. Microzonation for Soil Liquefaction Potential Using Simplified Methods, *In: Proceedings of the third international earthquake microzonation conference*, Seattle, WA, 3: 1319–30.

Javanbakht, A. 2019. Liquefaction Susceptibility Mapping of Western Metro Vancouver, UWO-ICLR-EMBC Stakeholder Engagement Workshop and Annual Update, Vancouver, BC, 11 Dec 2019, one map sheet.

Javanbakht, A., Molnar S.E. and Sadrekarimi, A. 2021. Liquefaction Hazard Mapping Using Geostatistical Method in Richmond, British Columbia, Canada, *17th World Conference on Earthquake Engineering*, Sept. 28-October 2, 2021, Sendai, Japan, Paper No: 4625, 12 pgs.

Kim, H.S., Kim, M., Laurie, G.B. and Kim, B. 2020. Local and Regional Evaluation of Liquefaction Potential Index and Liquefaction Sseverity Number for Liquefaction-Induced Sand Boils in Pohang, South Korea, *Soil Dyn Earthq Eng.*, 7:24.

Kolaj, M., Halchuk, S., Adams, J. and Allen, T.I. 2020. Sixth Generation Seismic Hazard Model of Canada: input files to produce values proposed for the 2020 National Building Code of Canada. Geological Survey of Canada, Open File 8630,: 15.

Lenz, J.A and Baise, L.G. 2007. Spatial Variability of Liquefaction Potential in Regional Mapping Using CPT and SPT data, *Soil Dynamics and Earthquake Engineering*. 27, 690–702.

Luna, R. and Frost, J.D. 1998. Spatial Liquefaction Analysis System, *J Comput CivEng*, 12 (1): 48–56.

Molnar, S.E., Assaf, J., Sirohey, A. and Adhikari, S.R. 2020. Overview of Local Site Effects and Seismic Microzonation Mapping in Metropolitan Vancouver, British Columbia, Canada, Engineering Geology, Special Issue on Seismic site response estimation for microzonation studies promoting the resilience of urban centers, 270 (5), 105568.

Monahan, A.P, Levson, V.M. and Kerr, B. 2010a. Liquefaction Hazard Map of Richmond, British Columbia. Geoscience Map 2010-3.

Monahan, A.P., Levson, V.M. and Kerr, B. 2010b. Quaternary Geology Map of Richmond, British Columbia, British Columbia Geological Survey, Geoscience Map 2010-2. (http://www.empr.gov.bc.ca/MINING/GEOSCIENCE/PUBLICATIONSCATALOGUE/MAPS/GEOSCIENCEMAPS/Pages/2010-2.aspx).

Papathanassiou, G., Valkaniotis, S., Chaztipetros, A. and Pavlides, S. 2017. Liquefaction Susceptibility Map of Greece, *Bull. Geol. Soc. Greece*, 43 (3): 1383–1392.

Rahman, M.Z., Siddiqua, S. and Kamal, ASMM. 2015. Liquefaction Hazard Mapping by Liquefaction Potential Index for Dhaka City, Bangladesh. *Eng Geol*, 188, 137–147.

Robertson, P.K. 2004. Evaluating Soil Liquefaction and Post-Earthquake Deformations Using CPT, *In: Proceedings of the second international conference on site characterization*, Porto, Portugal, 1: 233–49.

Robertson, P.K. 2009. Interpretation of Cone Penetration Tests – a Unified Approach, *Canadian Geotechnical Journal*, 46, 1337-1355.

Robertson P.K. and Cabal K.L. 2015. Guide to Cone Penetration Testing for Geotechnical Engineering, Gregg drilling. 6th edition.

Seed H.B. and Idriss I.M. 1971. Simplified Procedure for Evaluation Soil Liquefaction Potential, *Journal of the Soil Mechanics and Foundations Division*, ASCE 97, 1249–1273 SM9.

Sonmez, H. 2003. Modification of The Liquefaction Potential Index and Liquefaction Susceptibility Mapping for a Liquefaction-Prone Area (Inegol, Turkey), *Environ Geol*, 44 (7): 862–71.

Terzaghi, K. 1995. Evaluation of Coefficients of Subgrade Reaction, *Geotechnique*, 5(4): 297–326.

Toprak, S. and Holzer T.L. 2003. Liquefaction Potential Index: Field Assessment, *J Geotech Geoenviron Eng.*, 129 (4): 315–22.

Youd TL, Idriss IM, Andrus RD, Arango I, Castro G, Christian JT, et al. 2001. Liquefaction Resistance of Soils: Summary Report from the 1996 NCEER and 1998 NCEER/NSF workshops on Evaluation of Liquefaction Resistance of Soils, *J Geotech Geoenviron Eng*, 127 (10): 817–33.